Draft version November 4, 2020
Typeset using LaTeX **twocolumn** style in AASTeX63

Spectral and timing characterization of the X-ray pulsar XTE J1858+034 with NuSTAR and Fermi/GBM and a candidate cyclotron line

C. Malacaria,[1,2] P. Kretschmar,[3] K.K. Madsen,[4,5] C.A. Wilson-Hodge,[6] Joel B. Coley,[7,8] P. Jenke,[9] Alexander A. Lutovinov,[10] K. Pottschmidt,[8,5] Sergey S. Tsygankov,[11,10] and J. Wilms[12]

[1] *NASA Marshall Space Flight Center, NSSTC, 320 Sparkman Drive, Huntsville, AL 35805, USA**

[2] *Universities Space Research Association, Science and Technology Institute, 320 Sparkman Drive, Huntsville, AL 35805, USA*

[3] *European Space Agency (ESA), European Space Astronomy Centre (ESAC), Camino Bajo del Castillo s/n, 28692 Villanueva de la Cañada, Madrid, Spain*

[4] *CRESST and X-ray Astrophysics Laboratory, NASA Goddard Space Flight Center, Greenbelt, MD 20771, USA*

[5] *Department of Physics and Center for Space Science and Technology, University of Maryland, Baltimore County, Baltimore, MD 21250, USA*

[6] *ST 12 Astrophysics Branch, NASA Marshall Space Flight Center, Huntsville, AL 35812, USA*

[7] *Department of Physics and Astronomy, Howard University, Washington, DC 20059, USA*

[8] *CRESST and Astroparticle Physics Laboratory, NASA Goddard Space Flight Center, Greenbelt, MD 20771, USA*

[9] *University of Alabama in Huntsville (UAH), Center for Space Plasma and Aeronomic Research (CSPAR), 301 Sparkman Drive, Huntsville, Alabama 35899*

[10] *Space Research Institute of the Russian Academy of Sciences, Profsoyuznaya Str. 84/32, Moscow 117997, Russia*

[11] *Department of Physics and Astronomy, FI-20014 University of Turku, Finland*

[12] *Remeis-Observatory and Erlangen Centre for Astroparticle Physics, Friedrich-Alexander-Universität Erlangen-Nürnberg, Sternwartstr. 7, 96049 Bamberg, Germany*

ABSTRACT

Accreting X-ray pulsars (XRPs) undergo luminous X-ray outbursts during which the spectral and timing behavior of the neutron star can be studied in detail. We analyze a *NuSTAR* observation of the XRP XTE J1858+034 during its outburst in 2019. The spectrum is fit with a phenomenological, a semi-empirical and a physical spectral model. A candidate cyclotron line is found at 48 keV, implying a magnetic field of 5.4×10^{12} G at the site of emission. This is also supported by the physical best-fit model. A nominal *Gaia* distance of 1.55 kpc is available for a star that is close to – although not coincident with – the previously proposed optical counterpart but, based on *Fermi* Gamma-ray Burst Monitor data, the standard disk accretion-torque theory allowed us to infer a distance of 10.9 ± 1.0 kpc. Pulse profiles are single-peaked and show a pulsed fraction that is strongly energy-dependent at least up to 40 keV.

Keywords: X-ray binary stars – stars: neutron – pulsars: individual: XTE J1858+034 – accretion, accretion disks – magnetic fields

1. INTRODUCTION

Accreting X-ray pulsars (XRPs) are binary systems consisting of a neutron star (NS) which accretes matter originating from the stellar wind of the donor companion star. XTE J1858+034 is an XRP discovered with the *Rossi X-ray Timing Explorer (RXTE)* in 1998 by Remillard et al. (1998) and Takeshima et al. (1998). Those observations also detected X-ray pulsations with a period of ∼221 s. X-ray emission from this source has been detected only in a few short outbursts (Nakajima et al. 2019, and references therein), thus preventing to obtain an orbital solution or an in-depth characterization of the system. A Cyclotron Resonant Scattering Feature (CRSF) also was not observed from this source so far, thus the NS magnetic field strength is unknown. When observed, the energy $E_{\rm cyc}$ of the fundamental CRSF probes the magnetic field strength at the site of spectral emission, $E_{\rm cyc} \sim 11.6 \times B_{12}(1+z_{\rm g})^{-1}$ keV, where B_{12} is the magnetic field in units of 10^{12} G, and $z_{\rm g}$ is the gravitational redshift (see Staubert et al. 2019 for a recent review). However, Paul & Rao (1998) proposed a magnetic field strength of $0.8 \times 10^{12} \times d_{kpc}$ G (with d_{kpc} the

Corresponding author: cmalacaria@usra.edu
* NASA Postdoctoral Fellow

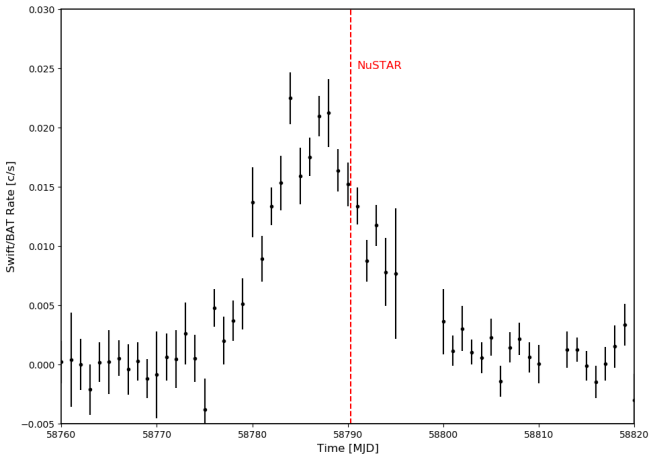

Figure 1. *Swift*/BAT daily average light curve of XTE J1858+034 during the outburst in 2019 (black dots). The *NuSTAR* observation time is also shown (red dashed line).

distance value in units of kpc), based on the observation of quasi-periodical oscillations in this system.

Reig et al. (2004, 2005) proposed a Be-type star for the optical counterpart, of which neither the spectral subtype nor the distance was found. This star was the only one within the X-ray error circle (Molkov et al. 2004) showing Hα emission. More recently, *Gaia* identified a different optical counterpart candidate, with a distance of 1.55 kpc (Bailer-Jones et al. 2018). However, this source has a large ($\sim 103''$) angular offset compared to the optical counterpart proposed by Reig et al. (2005).

Recently, the source has undergone a new outburst episode (Nakajima et al. 2019), and it was observed with *NuSTAR*. Here we study its spectral and timing characteristics and finally form a consistent general overview for the X-ray behaviour of XTE J1858+034. The analysis presented here is complemented by that proposed in an accompanying paper by Tsygankov et al. (subm.).

2. DATA REDUCTION

NuSTAR (Harrison et al. 2013) was launched in 2012. It is currently the only X-ray mission with a telescope able to focus hard X-rays above 10 keV. *NuSTAR* consists of two identical co-aligned telescopes that focus X-ray photons onto two independent Focal Plane Modules, FPMA and FPMB. At the focus of each telescope module are four (2×2) solid-state cadmium zinc telluride (CdZnTe) imaging detectors. These provide wide-band (3–79 keV) energy coverage with a FWHM of $18''$ and a spectral resolution of 400 eV at 10 keV.

NuSTAR observed XTE J1858+034 on 2019 November 3 (ObsID 90501348002, MJD 58790), during an outburst (see Fig. 1). The total exposure time was about 44 ks. *NuSTAR* data were reduced with `NUSTARDAS` v1.9.5 provided by the `HEASOFT` v6.27.2 and using the *CALDB* 20200526 (Madsen et al. 2020). Cleaned events were obtained following the standard *NuSTAR* guidelines. The resulting images are shown in Fig. 2. Source spectra were extracted through the `NUPRODUCTS` routine. The source extraction region was a $65''$ radius circular region centered on the source, while the background was extracted from a source-free region on the same detector with radii of 90 and $105''$ for FPMA and FPMB, respectively. We also verified that shifting the extraction regions in order to account for the offset between the images from the two modules does not significantly affect the results. However, in FPMB part of the source events fall on the chip gap between detectors 0 and 3, resulting in unaccounted loss of effective area. This, along with the fact that there are calibration issues with detector absorption component of detector 3 (priv. comm.), led us to exclude the entire detector 3 from the FPMB extraction region. We obtained the FPMB ARF from a $15''$ radius circular region centered on the source, which ensures that the detector absorption of detector 3 did not get included. Similarly, to avoid accidentally including the RMF from detector 3 during RMF generation the RMF for detector 0 was obtained directly from the CALDB (`nuBcutdet0_20100101v001`).

Spectral data were analyzed using `XSPEC` v12.11.0l (Arnaud 1996). *NuSTAR* data were used in the range $3 - 60$ keV ($3.5 - 60$ keV for FPMB), above which the background dominates. Spectra were rebinned to have at least 50 counts per bin.

3. RESULTS

3.1. *Spectral analysis*

The spectrum of XTE J1858+034 as observed by *NuSTAR* in November 2019 clearly shows a steep shape. FPMA and FPMB spectra have been fitted simultaneously, allowing for a cross-normalization factor. For the spectral fit, standard phenomenological and semi-empirical continuum models have been employed, namely two variants of the cutoff power-law model (`cutoffpl` and `highecut*pow` in `XSPEC`) and a Comptonization model of soft photons in a hot plasma (`compTT` in `XSPEC`, Titarchuk 1994), respectively. To obtain an acceptable fit, the `cutoffpl` and `highecut*pow` models need an additional component in the lower energy band, which has been modeled as a blackbody emission as found in other accreting XRPs (see, e.g., La Palombara & Mereghetti 2006). However, the blackbody temperature is high with respect to other XRPs, indicating that the phenomenological model is likely inadequate. Moreover, we also tested a purely-physical model of thermal and bulk Comptonization of the seed

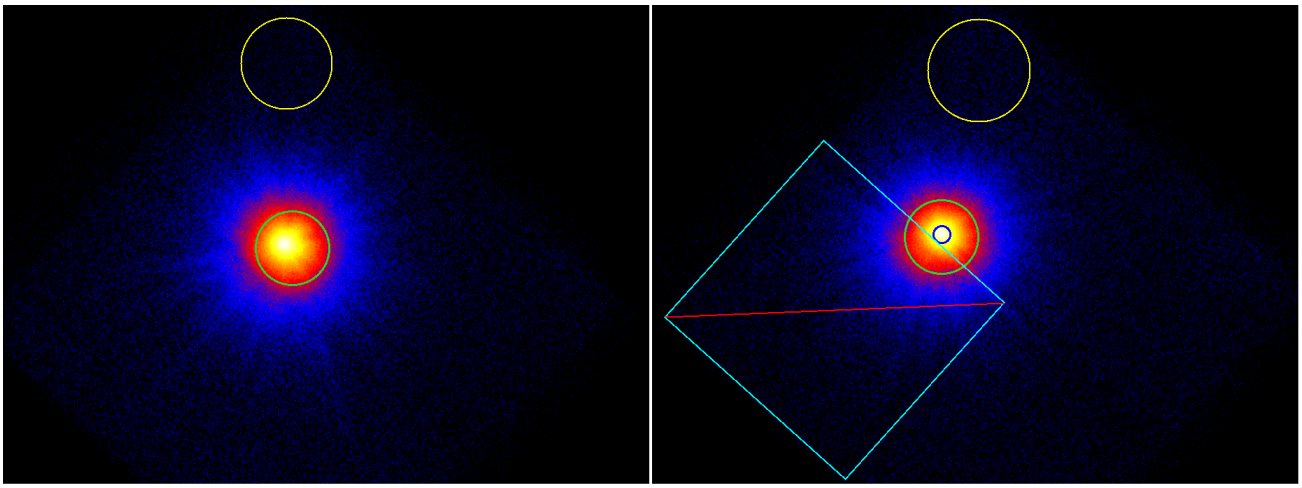

Figure 2. *NuSTAR* images of XTE J1858+034 as observed in November 2019 from FPMA (left) and FPMB (right). Circular green regions centered on the source represent the source extraction regions. Yellow solid circles on the top corner represent the background extraction regions. For FPMB, the blue small circle represents the ARF extraction region, while the barred cyan square represents the exclusion of detector 3 (see text). The color bar shows the number of counts per pixel.

photons produced by cyclotron cooling, Ferrigno et al. 2009 (`bwcycl` in `XSPEC`). For a fixed value of mass and radius of the accreting star, the `bwcycl` model has six free parameters, namely the accretion rate $\dot{M}$, the magnetic field strength B, the accretion column radius r_0, the electron temperature T_e, the photon diffusion parameter ξ and the Comptonization parameter δ. This model was successfully used to fit the broad-band energy spectrum of a number of bright ($\gtrsim 10^{37}\,\mathrm{erg\,s^{-1}}$) accreting XRPs (see, e.g., Epili et al. 2017; D'Aì et al. 2017; Wolff et al. 2016).

For all tested models, the photoelectric absorption component and elemental abundances were set according to Wilms et al. 2000 (`tbabs` in `XSPEC`) to account for photoelectric absorption by neutral interstellar matter (or column density N_H), and assuming model-relative (`wilm`) solar abundances. For reference, the Galactic N_H in the direction of the source is about $1.7 \times 10^{22}\,\mathrm{cm^{-2}}$ (HI4PI Collaboration et al. 2016). All tested models also were equipped with a Gaussian emission line at 6.4 keV to account for the Fe Kα fluorescence emission.

All fit continuum models show absorption-like residuals in the range $40 - 50$ keV. These residuals can be modeled with a Gaussian absorption line (see Fig. 3). The improvement in the best-fit statistics is maximum in the `compTT` model, i.e. $\Delta\chi^2 = 878$. Other models show an improvement of $\Delta\chi \gtrapprox 400$, with the lowest $\Delta\chi$ derived from the `highecut*pow` model. The significance of the line in the `compTT` model has been assessed through Monte Carlo simulations. For this task, the `XSPEC simftest` routine was adopted, which allows to simulate a chosen number of spectra based on the actual data and test the resulting $\Delta\chi^2$ between each instance fit with and without the model component in exam (the Gaussian absorption line in our case). Following Bhalerao et al. (2015); Bodaghee et al. (2016), the column density parameter was fixed to its best-fit value, and the energy and width of the Gaussian absorption line were left free to vary within their 90% confidence region in order to improve the speed and convergence of the fits. Simulations results are reported in Fig. 4 for a 10^4 iterations process and confirm the significance of the absorption feature at $> 3\sigma$ c.l. Following Marcu-Cheatham et al. (2015), we also investigated the impact of a variable background normalization on the absorption feature parameters. Using the `XSPEC` tool `recorn`, it was found that the absorption line parameters do not change significantly up to a 50% higher background level, thus strengthening the interpretation of the absorption feature as real and not due to artifacts. The feature was also observed in phase-resolved spectra presented in the accompanying paper by Tsygankov et al. (subm.). Interpreting the feature at 48 keV as a CRSF, and assuming a gravitational redshift of $z_g = 0.3$, a magnetic field strength of B$= (5.4 \pm 0.1) \times 10^{12}$ G is obtained.

Following the `bwcycl` model instructions[1], it is convenient to freeze some of the model parameters in order to help the computation of the best-fit parameters. Once the best-fit was found, the column density N_H was fixed to its best-fit value to help the fit converge and to ob-

[1] https://heasarc.gsfc.nasa.gov/xanadu/xspec/manual/node148.html.

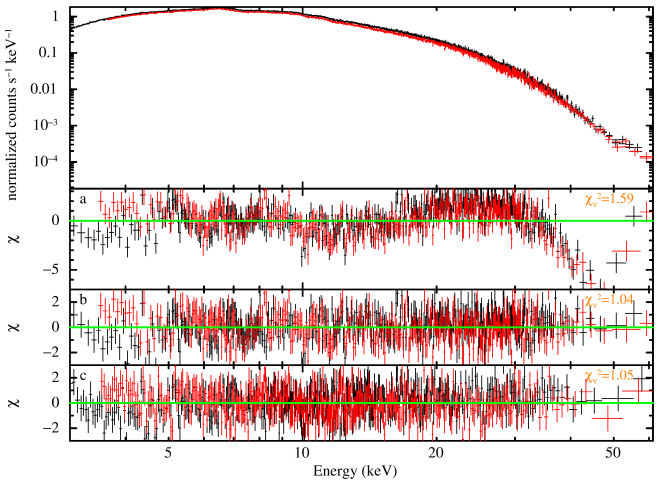

Figure 3. *Top*: XTE J1858+034 spectrum as observed by *NuSTAR* in 2019 and fit with a `ComptT` model. Lower panels are referred with a letter in the upper left corner. *Panel a*: residuals of the `ComptT` model. *Panel b*: residuals of the best-fit `ComptT` model including a Gaussian absorption line at $\sim$ 48 keV (see Table 1). *Panel c*: residuals of the best-fit `BWCYC IIa` model including a Gaussian absorption line at $\sim$ 48 keV (see Table 2). Spectra and residuals have been rebinned for plotting purpose. The orange text in the right corners of the lower panels shows the correspondent model χ^2 divided by ν degrees of freedom.

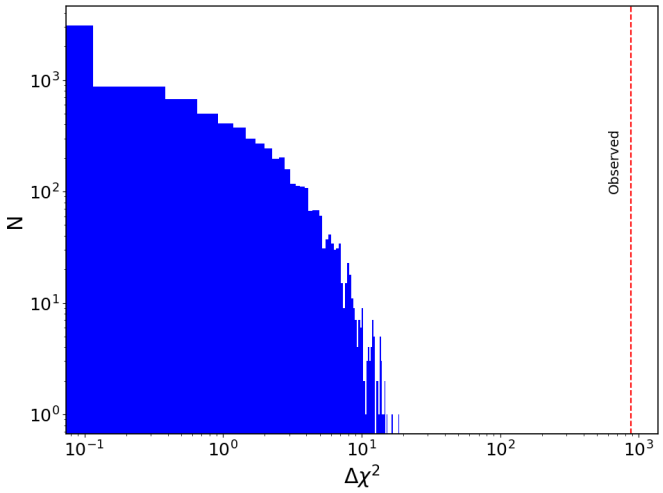

Figure 4. Results of 10000 Monte Carlo simulations to test the significance of the Gaussian absorption line in the `CompTT` model. The solid histogram shows the frequency (y-axis) of $\Delta\chi^2$ values (x-axis) obtained in the simulation. The red dashed line shows the observed $\Delta\chi^2 = 878$.

tain parameters errors. Mass and radius of the NS were fixed to their canonical values of 1.4$M_\odot$ and 10 km, respectively. However, it is preferable to also fix the values of the NS magnetic field, its distance and its mass accretion rate (as derived by the observed luminosity). For XTE J1858+034, there are no previous estimations of the magnetic field, while a measurement of the distance is necessary for the latter two parameters. The *Gaia* Data Release 2 (DR2, Gaia Collaboration et al. 2018) finds the XTE J1858+034 closest optical counterpart at an angular offset of $\sim 103''$ from the counterpart proposed by Reig et al. (2005). *Gaia*'s counterpart has a distance value of $1.55^{+0.28}_{-0.21}$ kpc. However, as already noticed in Malacaria et al. (2020), the *Gaia* distance does not match with accretion-torque expectations (see Fig. 5 of their work). Therefore, different configurations of the model have been tested (see Table 2).

First, a distance of 1.55 kpc was tested in the `bwcycl` model, along with a mass accretion rate $\dot{M} = 2.4 \times 10^{15}\,\mathrm{g\,s^{-1}}$ derived assuming a luminosity $L = \eta \dot{M} c^2$, with efficiency $\eta = 0.2$ (Sibgatullin & Sunyaev 2000), and c the speed of light. For this model configuration, the magnetic field strength also was tested as a free parameter (`BWCYC Ia`), and by fixing its value to $B = 5.4 \times 10^{12}$ G (`BWCYC Ib`). However, the latter configuration (Ib) was found unable to fit the data. Alternatively, a model configuration with $B = 5.4 \times 10^{12}$ G, $d = 1.55$ kpc and $\dot{M}$ left as a free parameter also fits the data (`BWCYC Ic`), but the resulting $\dot{M}$ value is about five times higher than that assumed in `BWCYC Ic` (see Table 2).

Second, a different configuration of the model was tested, based on a distance value inferred from the spin-up ($\dot{P}$) measured by Fermi-GBM. To this aim, the publicly available spin-frequency values from GBM were used. The spin-up was measured during an interval of about 6 days around MJD 55458. The resulting spin-up value is $|\dot{P}| = 10.5421(6)\,\mathrm{s\,yr^{-1}}$ (see also Malacaria et al. 2020, and references therein). Since the orbital parameters of this system are unknown, we tested the contribution of orbital modulation to the observed spin-up. First, a visual inspection of the *Swift*/BAT data for this source revealed an outbursts recurrence of $\sim$81 days, here assumed as the orbital period. Moreover, a value of the mass function $f(M) = {M_*}^3 sin^3 i/(M_* + M_{NS})^2 = 10$ was assumed, where M_* and M_{NS} are the mass of the companion and that of the NS, respectively, i is the binary system inclination. This value was chosen to maximize the semi-major projected axis, $a_x\, sin\, i = 400$ l-s which, together with an eccentricity value as high as $e = 0.8$, in turn maximize the orbital signature on the observed spin frequency. Finally, an epoch of $T0 = 53436$ MJD was chosen at the beginning of the first of the recurring outbursts. An argument of periapse of $\omega = 195°$ was found to best-fit the GBM frequency values assuming no accretion torque. Despite all the assumptions, a spin-period derivative of about 11 $\mathrm{s\,yr^{-1}}$

Table 1. Best-fit results of XTE J1858+034 spectral analysis with a cutoff power-law model `cutoffpl` and a Comptonization model `CompTT`. All reported errors are at 1σ c.l.

	cutoffpl	CompTT
C_{FPMB}	$0.747^{+0.001}_{-0.001}$	$0.747^{+0.001}_{-0.001}$
N_H [10^{22} cm^{-2}]	$7.6^{+0.4}_{-0.4}$	$5.8^{+0.3}_{-0.3}$
kT_{bb} [keV]	$5.2^{+0.2}_{-0.1}$	–
$norm_{bb}$	$0.0152^{+0.0002}_{-0.0007}$	–
$E_{K\alpha}$ [keV]	$6.47^{+0.02}_{-0.02}$	$6.48^{+0.02}_{-0.02}$
$\sigma_{K\alpha}$ [keV]	$0.26^{+0.02}_{-0.02}$	$0.28^{+0.02}_{-0.02}$
$norm_{K\alpha}$ (10^{-4})	$5.5^{+0.4}_{-0.4}$	$5.9^{+0.4}_{-0.4}$
Γ	$0.03^{+0.29}_{-0.22}$	–
HighECut [keV]	$3.5^{+1.5}_{-0.5}$	–
$norm_\Gamma$*	$0.025^{+0.006}_{-0.004}$	–
T0 [keV]	–	$1.02^{+0.02}_{-0.02}$
kT_{CompTT} [keV]	–	$5.61^{+0.05}_{-0.04}$
τ_p [keV]	–	$7.07^{+0.06}_{-0.06}$
$norm_{CompTT}$	–	$0.0228^{+0.0003}_{-0.0003}$
E_{gabs} [keV]	$46.8^{+1.0}_{-0.8}$	$48.0^{+0.8}_{-0.7}$
σ_{gabs} [keV]	$7.7^{+1.0}_{-0.7}$	$8.6^{+0.6}_{-0.5}$
Strength$gabs$	$14.9^{+5.1}_{-2.6}$	$21.3^{+2.0}_{-2.5}$
Flux†	$1.499^{+0.003}_{-0.003}$	$1.499^{+0.003}_{-0.003}$
χ^2/d.o.f.	1645/1574	1643/1573

* In units of photons/keV/cm^2/s at 1 keV. † Flux calculated for the entire model in the 3−60 keV band and reported in units of 10^{-9} erg cm^{-2} s^{-1}. Flux values with estimated errors were derived using the `cflux` model from `XSPEC` as resulting from FPMA.

is still required to fit the data. We therefore conclude that the orbital contribution to the measured $\dot{P}$ is not significant.

Assuming a magnetic field strength of 5.4×10^{12} G and adopting the *NuSTAR* measured flux of 1.5×10^{-9} erg cm^{-2} s^{-1} (see Table 1 and 2), the standard accretion-disk torque theory (Ghosh & Lamb 1979) for a $|\dot{P}| = 10.5$ s yr^{-1} allows to infer a distance of $d = 10.9 \pm 1.0$ kpc (estimated uncertainty at 1σ c.l.). This distance value is also independently confirmed by the analysis of the optical companion star as reported in the accompanying paper by Tsygankov et al. (subm.). A distance of $d = 10.9$ kpc was used to characterize a different set of configurations of the `bwcyc` model. The corresponding $\dot{M} = 1.2 \times 10^{17}$ g s^{-1} was adopted altogether. The model was tested with the magnetic field strength as a free parameter (`BWCYC IIa`) and as fixed to 5.4×10^{12} G (`BWCYC IIb`). For comparison with `BWCYC Ic`, a model configuration with a free $\dot{M}$ (and a fixed magnetic field strength) was also tested (`BWCYC IIc`).

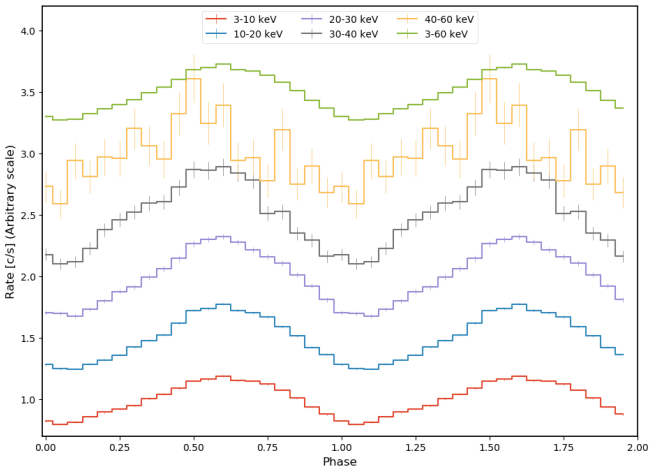

Figure 5. XTE J1858+034 energy-resolved pulse profiles as observed by *NuSTAR*. The energy band increases upwards. Pulse profiles are shown twice in phase and rescaled in count rate for clarity.

3.2. *Timing analysis*

For the timing analysis, the `nuproducts` task was used to obtain light curves out of calibrated and cleaned events. These light curves were corrected for livetime, exposure and vignetting effects, and were extracted in the following energy bands: $3-10$, $10-20$, $20-30$, $30-40$, $40-60$ and $3-60$ keV.

All light curves were barycentered using the `barycorr` tool and the *NuSTAR* clock correction file `nuCclock20100101v103`. The light curve in the $3-60$ keV energy band was binned to 5 s and used to search for pulsations around the known 221 s periodicity with the epoch folding method (Leahy 1987). The procedure results in a measured period of $P = 218.393(2)$ s. The uncertainty was estimated by simulating 500 light curves based on real data and altered with Poisson noise.

Light curves in different energy bands were folded to the best-fit spin period to obtain pulse profiles with a resolution of 20 phase bins (see Fig. 5). In turn, these were used to explore the pulsed fraction variation as a function of the energy (see Fig. 6). The pulsed fraction here is defined as $(I_{max} - I_{min})/(I_{max} + I_{min})$, where I_{max}, I_{min} are the maximum and minimum pulse profile count rate, respectively.

4. DISCUSSION

4.1. *Thermal Comptonization and a candidate cyclotron line*

The hard spectrum of XTE J1858+034 resembles that of other accreting X-ray pulsars observed both at low

Table 2. Best-fit results of XTE J1858+034 spectral analysis with different configurations of the physical Bulk+Thermal Comptonization model `bwcyc`. `BWCYC Ia, Ic` have the distance value fixed at the source's *Gaia* closest counterpart $d = 1.55$ kpc (`BWCYC Ib` does not fit the data, see text, and is therefore not included in this table). `BWCYC IIa, IIb, IIc` have the distance value fixed at $d = 10.9$ kpc. All reported errors are at 1σ c.l.

	BWCYC Ia ($d, \dot{M}$ fixed, B free)	BWCYC Ic (d, B fixed, $\dot{M}$ free)	BWCYC IIa ($d, \dot{M}$ fixed, B free)	BWCYC IIb ($d, B, \dot{M}$ fixed)	BWCYC IIc (d, B fixed, $\dot{M}$ free)
C_{FPMB}	$0.747^{+0.001}_{-0.001}$	$0.747^{+0.001}_{-0.001}$	$0.748^{+0.001}_{-0.001}$	$0.748^{+0.001}_{-0.001}$	$0.748^{+0.001}_{-0.001}$
N_H [10^{22} cm^{-2}]	$7.4^{+0.5}_{-0.6}$	$8.2^{+0.3}_{-0.2}$	$8.6^{+0.2}_{-0.2}$	$8.4^{+0.2}_{-0.2}$	$8.4^{+0.3}_{-0.8}$
$E_{K\alpha}$ [keV]	$6.47^{+0.02}_{-0.02}$	$6.47^{+0.02}_{-0.02}$	$6.47^{+0.02}_{-0.02}$	$6.48^{+0.02}_{-0.02}$	$6.47^{+0.02}_{-0.02}$
$\sigma_{K\alpha}$ [keV]	$0.29^{+0.02}_{-0.02}$	$0.27^{+0.02}_{-0.02}$	$0.27^{+0.02}_{-0.02}$	$0.28^{+0.02}_{-0.02}$	$0.27^{+0.02}_{-0.02}$
norm$_{K\alpha}$ (10^{-4})	$6.1^{+0.4}_{-0.3}$	$5.4^{+0.4}_{-0.2}$	$5.5^{+0.4}_{-0.4}$	$5.6^{+0.3}_{-0.3}$	$5.6^{+0.4}_{-0.4}$
ξ	$19.9^{*}_{-10.9}$	$2.5^{+1.0}_{-0.5}$	$4.2^{+0.7}_{-1.7}$	$3.2^{+0.8}_{-0.8}$	$2.9^{+1.0}_{-0.6}$
δ	$(5.06^{+7.8}_{-0.08})$E-2	$0.8^{+0.4}_{-0.4}$	$0.4^{+0.3}_{-0.1}$	$0.6^{+0.3}_{-0.1}$	$0.7^{+0.3}_{-0.2}$
B [10^{12} G]	$0.15^{+0.02}_{-0.01}$	5.4 (fixed)	$4.4^{+0.5}_{-0.3}$	5.4 (fixed)	5.4 (fixed)
$\dot{M}$ [10^{17} g/s]	0.024 (fixed)	$0.12^{+0.01}_{-0.02}$	1.2 (fixed)	1.2 (fixed)	$1.1^{+0.1}_{-0.1}$
T_e [keV]	$5.81^{+0.05}_{-0.12}$	$5.4^{+0.2}_{-0.6}$	$5.6^{+0.2}_{-0.6}$	$5.5^{+0.1}_{-0.5}$	$5.2^{+0.2}_{-0.4}$
r_0 [m]	$208.5^{+12.3}_{-80.5}$	$14.3^{+7.0}_{-14.3}$	73^{+9}_{-22}	66^{+22}_{-12}	49^{+29}_{-10}
d [kpc]	1.55 (fixed)	1.55 (fixed)	10.9 (fixed)	10.9 (fixed)	10.9 (fixed)
E_{gabs} [keV]	$48.5^{+0.8}_{-0.7}$	$48.2^{+1.0}_{-1.4}$	$48.3^{+0.7}_{-0.7}$	$48.6^{+0.5}_{-1.3}$	$48.3^{+1.0}_{-1.1}$
σ_{gabs} [keV]	$9.2^{+0.5}_{-0.5}$	$9.2^{+3.1}_{-0.8}$	$10.3^{+0.7}_{-2.1}$	$9.6^{+1.2}_{-1.2}$	$9.3^{+1.3}_{-0.6}$
Strength$_{gabs}$	$25.9^{+2.8}_{-2.6}$	$24.3^{+4.5}_{-7.5}$	$25.4^{+4.2}_{-6.4}$	$27.6^{+3.1}_{-4.2}$	$25.3^{+4.0}_{-3.9}$
Flux†	$1.499^{+0.003}_{-0.003}$	$1.499^{+0.003}_{-0.003}$	$1.499^{+0.003}_{-0.003}$	$1.499^{+0.003}_{-0.002}$	$1.499^{+0.003}_{-0.003}$
χ^2/d.o.f.	1653/1574	1648/1574	1648/1574	1648/1575	1648/1574

* unconstrained. † Flux calculated in the $3-60$ keV band and reported in units of 10^{-9} erg cm^{-2} s^{-1}. Flux values with estimated errors were derived using the `cflux` model from `XSPEC` as calculated for FPMA.

and high luminosity and well fit by a `CompTT` model (Mukerjee et al. 2020, and references therein). The observation of `CompTT` spectra in accreting X-ray pulsars is usually interpreted as the result of thermal Comptonization processes in which the thermal energy of the accreting gas is transferred to the seed photons originating from the NS hotspots (Becker & Wolff 2007). An increasing number of these sources also show that an additional `CompTT` component emerges in the high-energy range of the spectrum at low-luminosity stages (Tsygankov et al. 2019a,b). Although the formation of such component is not clear yet, it is likely due to a combination of cyclotron emission and following thermal Comptonized emission from a thin overheated layer of the NS atmosphere (see Tsygankov et al. 2019b, and references therein). In this context, X Persei is a remarkable case since it has been shown that the cyclotron line in its spectrum can be mimicked by the convolution of the two `CompTT` spectral components around the energy where the flux from the low- and high-energy components is comparable (Doroshenko et al. 2012). However, among the sources whose spectrum is formed by two `CompTT` components, X Persei is the one with the highest electron temperature of the hard-energy `CompTT` component, $kT \sim 15$ keV. If the absorption feature at ~ 48 keV in XTE J1858+034 is in fact resulting from the blend of two `CompTT` components, the high-energy `CompTT` would peak around 22 keV. This would make XTE J1858+034 the most extreme among the X-ray pulsars that show such spectral shape. Moreover, such a spectral shape has so far only been observed in low-luminosity X-ray pulsars. This would be the case for XTE J1858+034 if the *Gaia* distance of $d = 1.55$ kpc is the true distance. However, the analysis reported in Sect. 3.1 shows that a distance of 10.9 kpc is more consistent with X-ray observations of the spin period derivative, as well as with the study of the optical companion performed by Tsygankov et al. (subm.). A second Gaussian or `CompTT` component that peaked above 45 keV was also tested in place of the absorption feature, but could not be successfully fit ($\chi^2_{red} > 1.4$), although possibly due to the lack of statistics above 60 keV. In the following section we discuss the scenarios of spectral formation for the low- and high-luminosity cases ($d = 1.55$ and 10.9 kpc, respectively).

4.2. *Thermal and bulk Comptonization*

Dealing with two different possible values of the source distance, two different configurations of the `BWcyc` model have been tested in this work.

If XTE J1858+034 distance is $d = 1.55\,\mathrm{kpc}$, the derived flux of $1.5\times10^{-9}\,\mathrm{erg\,cm^{-2}\,s^{-1}}$ (see Table 1) implies a luminosity of $4.3\times10^{35}\,\mathrm{erg\,s^{-1}}$. In this case, the `BWCYC Ia` fit returns anomalous values of the ξ and δ parameters and an unexpectedly low magnetic field strength ($1.5\times10^{11}\,\mathrm{G}$). On the other hand, the `BWCYC Ic` fit returns a column radius value r_0 that is consistent with zero, and the model needs a mass accretion rate $\dot{M}$ that is about 5 times larger than that inferred from the X-ray (isotropic) luminosity. A `BWCYC Ib` model configuration with distance, magnetic field strength and $\dot{M}$ fixed to their expected values do not fit the data.

On the other hand, if the source distance is $d = 10.9\,\mathrm{kpc}$, the derived flux of $1.5\times10^{-9}\,\mathrm{erg\,cm^{-2}\,s^{-1}}$ implies a luminosity of $2.1\times10^{37}\,\mathrm{erg\,s^{-1}}$. In this case, all configurations of the `bwcyc` model are statistically equivalent and all parameters show acceptable values. For the `BWCYC IIa` configuration, the returned magnetic field strength of $4.2\times10^{12}\,\mathrm{G}$ is consistent within 2σ with that inferred from the candidate CRSF. Contrary to the case with $d = 1.55\,\mathrm{kpc}$, the `BWCYC IIb` model fits the data and also returns acceptable values of the fit parameters. The `BWCYC IIc` fit returns the smallest (but still acceptable) r_0 value, and a mass accretion rate $\dot{M}$ that is almost coincident with that inferred from the X-ray (isotropic) luminosity.

In any case, when interpreting the results from the `BWcyc` model, it is important to keep in mind that, as reported in Ferrigno et al. (2009), the `BWcyc` model may need adjustments in the spectral parameters with respect to the original prescriptions. For example, the best-fit magnetic field value may differ from that inferred by the CRSF if the spectrum is formed at a NS site that is spatially different than the CRSF forming region. Likewise, the best-fit mass accretion rate $\dot{M}$ can be different from that inferred by the X-ray luminosity due to an uncertain efficiency conversion factor (η) and anisotropic emission.

4.3. *Timing results*

Pulse profiles of XTE J1858+034 as observed by *NuSTAR* show a single-peak structure and a shape that is only weakly energy-dependent (see Fig. 5). This is typically observed at low mass accretion rates (see, e.g. Malacaria et al. 2015), and qualitatively interpreted as the beaming pattern resulting from a pencil-beam emission. However, single-peaked pulse profiles are also observed at high accretion rates, like in the case of Pulsating Ultra-Luminous X-ray sources (PULXs), e.g. Swift J0243.6+6124, where single-peak pulse profiles persist at high luminosity and only switch to more complex profiles at super-Eddington luminosity (Wilson-Hodge et al. 2018).

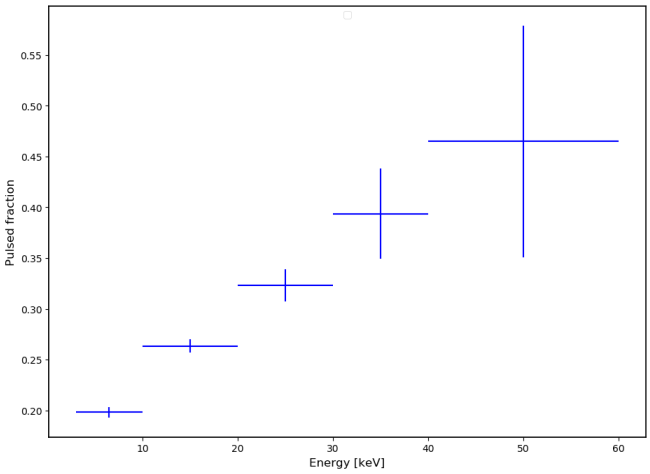

Figure 6. XTE J1858+034 pulsed fraction as a function of the energy during the *NuSTAR* observation in November 2019.

The pulsed fraction shows a considerable energy-dependence, and almost doubles from 20% in the $3-10\,\mathrm{keV}$ to about 40% in the $30-40\,\mathrm{keV}$ energy band, above which the lack of statistics prevent us from drawing firm conclusions.

5. CONCLUSIONS

We analyzed the *NuSTAR* observation of the 2019 outburst of the BeXRB XTE J1858+034. The source, relatively poorly studied, has now been characterized in different ways. A candidate cyclotron line is found in its spectrum at 48 keV. This implies a magnetic field strength of $5.4\times10^{12}\,\mathrm{G}$, consistent with the value obtained from the physical fitting model of thermal and bulk Comptonization `bwcyc` in its best-fit configurations. Arguments are given to review the previously proposed optical counterpart and its distance value in favor of a distance of $10.9\pm1.0\,\mathrm{kpc}$ obtained from standard accretion-torque theory.

ACKNOWLEDGMENTS

This research has made use of data and software provided by the High Energy Astrophysics Science Archive Research Center (HEASARC), which is a service of the Astrophysics Science Division at NASA/GSFC and the High Energy Astrophysics Division of the Smithsonian Astrophysical Observatory. We acknowledge extensive

use of the NASA Abstract Database Service (ADS). C.M. is supported by an appointment to the NASA Postdoctoral Program at the Marshall Space Flight Center, administered by Universities Space Research Association under contract with NASA. AAL and SST acknowledge support from the Russian Science Foundation (grant 19-12-00423).

REFERENCES

Arnaud, K. A. 1996, in Astronomical Society of the Pacific Conference Series, Vol. 101, Astronomical Data Analysis Software and Systems V, ed. G. H. Jacoby & J. Barnes, 17

Bailer-Jones, C. A. L., Rybizki, J., Fouesneau, M., Mantelet, G., & Andrae, R. 2018, AJ, 156, 58

Becker, P. A., & Wolff, M. T. 2007, ApJ, 654, 435

Bhalerao, V., Romano, P., Tomsick, J., et al. 2015, MNRAS, 447, 2274

Bodaghee, A., Tomsick, J. A., Fornasini, F. M., et al. 2016, ApJ, 823, 146

D'Aì, A., Cusumano, G., Del Santo, M., La Parola, V., & Segreto, A. 2017, MNRAS, 470, 2457

Doroshenko, V., Santangelo, A., Kreykenbohm, I., & Doroshenko, R. 2012, A&A, 540, L1

Epili, P., Naik, S., Jaisawal, G. K., & Gupta, S. 2017, MNRAS, 472, 3455

Ferrigno, C., Becker, P. A., Segreto, A., Mineo, T., & Santangelo, A. 2009, A&A, 498, 825

Gaia Collaboration, Brown, A. G. A., Vallenari, A., et al. 2018, A&A, 616, A1

Ghosh, P., & Lamb, F. K. 1979, ApJ, 234, 296

Harrison, F. A., Craig, W. W., Christensen, F. E., et al. 2013, ApJ, 770, 103

HI4PI Collaboration, Ben Bekhti, N., Flöer, L., et al. 2016, A&A, 594, A116

La Palombara, N., & Mereghetti, S. 2006, A&A, 455, 283

Leahy, D. A. 1987, A&A, 180, 275

Madsen, K. K., Grefenstette, B. W., Pike, S., et al. 2020, arXiv e-prints, arXiv:2005.00569

Malacaria, C., Jenke, P., Roberts, O. J., et al. 2020, ApJ, 896, 90

Malacaria, C., Klochkov, D., Santangelo, A., & Staubert, R. 2015, A&A, 581, A121

Marcu-Cheatham, D. M., Pottschmidt, K., Kühnel, M., et al. 2015, ApJ, 815, 44

Molkov, S. V., Cherepashchuk, A. M., Revnivtsev, M. G., et al. 2004, ATel, 274, 0

Mukerjee, K., Antia, H. M., & Katoch, T. 2020, arXiv e-prints, arXiv:2005.14044

Nakajima, M., Negoro, H., Kurogi, K., et al. 2019, The Astronomer's Telegram, 13217, 1

Paul, B., & Rao, A. R. 1998, A&A, 337, 815

Reig, P., Kougentakis, T., & Papamastorakis, G. 2004, ATel, 308, 0

Reig, P., Negueruela, I., Papamastorakis, G., Manousakis, A., & Kougentakis, T. 2005, A&A, 440, 637

Remillard, R., Levine, A., Takeshima, T., et al. 1998, IAUC, 6826, 0

Sibgatullin, N. R., & Sunyaev, R. A. 2000, Astronomy Letters, 26, 699

Staubert, R., Trümper, J., Kendziorra, E., et al. 2019, A&A, 622, A61

Takeshima, T., Corbet, R. H. D., Marshall, F. E., Swank, J., & Chakrabarty, D. 1998, IAUC, 6826, 0

Titarchuk, L. 1994, ApJ, 434, 570

Tsygankov, S. S., Doroshenko, V., Mushtukov, A. e. A., et al. 2019a, MNRAS, 487, L30

Tsygankov, S. S., Rouco Escorial, A., Suleimanov, V. F., et al. 2019b, MNRAS, 483, L144

Wilms, J., Allen, A., & McCray, R. 2000, ApJ, 542, 914

Wilson-Hodge, C. A., Malacaria, C., Jenke, P. A., et al. 2018, ApJ, 863, 9

Wolff, M. T., Becker, P. A., Gottlieb, A. M., et al. 2016, ApJ, 831, 194